Catalysis Science & Technology

PAPER

View Article Online
View Journal | View Issue

Cite this: *Catal. Sci. Technol.*, 2016, **6**, 5124

Encapsulation of chiral Fe(salen) in mesoporous silica structures for use as catalysts to produce optically active sulfoxides†

Rafael L. Oliveira,[ab] Tom Nijholt,[a] Mozaffar Shakeri,[a] Petra E. de Jongh,[a] Robertus J. M. Klein Gebbink[c] and Krijn P. de Jong*[a]

Received 16th January 2016,
Accepted 22nd February 2016

DOI: 10.1039/c6cy00113k

www.rsc.org/catalysis

Solid catalysts which are heterogeneous at the macroscopic scale but homogeneous at the microscopic level were prepared by the encapsulation of Fe(salen) by a "ship in a bottle" approach. This approach permits the synthesis of a "free" Fe(salen) complex inside the nanocages of SBA-16 and m-MCF, having conformational freedom and behaving as a complex in solution. These materials were used as catalysts for asymmetric oxidation of sulfides. The entrance sizes of the mesoporous materials SBA-16 and m-MCF were tuned by changing the synthesis parameters and by silylation of the silica surface with *n*-propyl groups, which resulted in materials with different Fe(salen) loadings. Chiral Fe(salen) trapped in m-MCF materials showed higher activity than the complex immobilized on SBA-16. The activity and enantioselectivity of the catalysts based on m-MCF were on a par with the homogeneous counterpart under specific conditions. The heterogenized catalysts presented a limited recyclability; however, they were clearly advantageous compared to the homogenous counterpart, where reutilization was not possible.

Introduction

Asymmetric oxidation of sulfides is an important method to produce optically active sulfoxides. These sulfoxides are widely used as chiral auxiliaries in asymmetric synthesis[1] and as bioactive molecules in the pharmaceutical industry, for example, drugs for treatment of platelet aggregation, neurodegenerative disorders, peptic ulcer diseases and others.[2] In the last few decades, several methods to produce enantiopure sulfoxides have been described; the use of biocatalysts and chiral metal complexes are the most applied methodologies.[3]

Chiral metal complexes based on titanium, vanadium and manganese have been extensively investigated.[4] In contrast, chiral iron complexes have been less explored for this reaction. Recently, much effort has been done to produce iron complexes for asymmetric oxidation of sulfides[5] since iron shows advantages such as low toxicity and earth abundance. Bryliakov *et al.* showed that Fe(salen) complexes can be used as catalysts for the asymmetric oxidation of sulfides; however, reasonable stereoselectivity was only obtained when iodosylbenzene was used as an external oxidant.[6] Egami *et al.* synthesized an Fe(salan) complex that showed good yield and stereoselectivity when H_2O_2 was used as an oxidant.[7]

Despite the catalytic performance of some chiral metal complexes, most of them have not been applied on an industrial scale yet. The major problems are the difficulty in separation, recycling and contamination with the metal of the desired products. Heterogeneous catalysts have attracted much attention due to their advantages, easy separation from the products and recyclability.[8] Thus, a lot of energy has been spent on the immobilization of metal complexes on solid supports, such as silica, polymers and carbon.[9] However, heterogeneous catalysts can suffer from degradation of the immobilized complexes and metal leaching, limiting their recyclability.[10] For example, Basset *et al.* studied a silica-supported zirconium complex applied on transesterification of acrylates and observed a considerable deactivation of the catalyst due to exchange of ligands during catalytic performance and also leaching of zirconium.[11]

Chiral complexes can be immobilized on solid matrixes using various methods, such as grafting, electrostatic interaction, sol–gel methods and encapsulation through a "ship in the bottle" approach.[12] In the "ship in the bottle" approach, metal complexes are usually synthesized inside porous materials such as zeolites.[13] The potential advantage of this approach is that the complex does not suffer modification, having the possibility to keep the same catalytic activity of the homogeneous counterpart. However, zeolites present some limitations as supports due to their small cage sizes and

[a] *Inorganic Chemistry and Catalysis, Debye Institute for Nanomaterials Science, Utrecht University, Netherlands. E-mail: k.p.dejong@uu.nl*
[b] *Institute of Chemistry, State University of Campinas, Brazil*
[c] *Organic Chemistry and Catalysis, Debye Institute for Nanomaterials Science, Utrecht University, Netherlands*

† Electronic supplementary information (ESI) available. See DOI: 10.1039/c6cy00113k

restricted window sizes, resulting often in materials with lower activity and stereoselectivity. Ordered mesoporous silica (OMS) has been shown as an alternative due to its larger entrance size and pore structure, permitting encapsulated complexes with more conformational freedom and behaving as a free complex in solution.[14] The most applied OMS for the "ship in the bottle" synthesis is SBA-16; nevertheless, it is difficult to obtain this material with large cage sizes (>7 nm) and small entrance sizes (~2 nm). Recently, our group reported the synthesis of a new silica material called modified mesocellular foam (m-MCF), which combines large cage sizes (15–22 nm) and narrow entrance sizes (1.8–3.7 nm), showing properties that are very interesting for application in the "ship in the bottle" approach.[15]

In this contribution, we encapsulated an Fe(salen) complex in modified m-MCF and SBA-16 materials with different entrance and cage sizes. m-MCF and SBA-16 surfaces were functionalized with *n*-propyl groups which allowed us to tune their entrance and cage sizes. The obtained hybrid materials were conveniently characterized to appraise the influence of their different structures on the loading of the Fe(salen) complex, and were evaluated as catalysts in asymmetric sulfoxidation, using the oxidation of thioanisole as a model reaction.

Experimental section

Chemicals

Triblock copolymer poly(ethylene oxide)–poly(propylene oxide)–poly(ethylene oxide) (P123), Pluronic F-127, tetraethyl orthosilicate (TEOS, 98%), *n*-propyltriethoxysilane (97%), mesitylene (TMB, 99%), styrene (99.5%), ethylene glycol (99%), methyl phenyl sulfoxide (97%) and iron(III) chloride hexahydrate ($FeCl_3{\cdot}6H_2O$, 97%) were purchased from Sigma Aldrich. Hydrogen peroxide (H_2O_2, 35 wt% in H_2O), acetonitrile (CH_3CN, HPLC), thioanisole (PhSMe, 99%), and methyl sulfoxide (DMSO, 99.7%) were purchased from Acros Organics. Benzyl phenyl sulfide ($PhSCH_2Ph$, 98%), 3,5-di-*tert*-butyl-2-hydroxybenzaldehyde (99%) and 1-butylamine (99%) were purchased from Alpha Aesar. (1*R*,2*R*)-Diaminocyclohexane (99%) was purchased from ABCR. Hydrochloric acid (HCl, 37%) was purchased from Emsure. Methanol (MeOH, 100%), ethanol (EtOH, 100%), dichloromethane (DCM, 99.5%), chloroform ($CHCl_3$, 99.5%) and toluene (100%) were purchased from Interchema.

Synthesis of materials and heterogenized Fe-salen complexes

m-MCF synthesis. For m-MCF synthesis, 4 g of copolymer Pluronic P123 was dissolved in an aqueous acidic solution (150 ml, 1.6 M HCl) in a 500 mL polypropylene bottle at room temperature overnight. Then, 3 grams of TMB (mesitylene) was added to the reaction mixture at 35 °C dropwise and stirred vigorously for 2 h. After this period, 17 grams of TEOS was slowly added to the mixture (1.5 mL min^{-1}) and stirred vigorously for 5 minutes. After this period, the mixture was kept under static conditions in the closed bottle at 35 °C for 20 hours followed by 24 hours at different temperatures 50°, 60°, 70°, and 80 °C. The solid product was collected by filtration, washed with distilled water, dried at 60 °C for 24 h and calcined at 550 °C in static air for 6 hours. The synthesized and calcined materials will be referred to as 'pristine materials' in this paper. The synthesized materials were designated as MCF-*X*, where *X* is the hydrothermal treatment temperature.

SBA-16 synthesis. The synthesis of SBA-16 was done, following the procedure described by Kim *et al.*[19] The structural properties of SBA-16 were tuned by changing the composition of the mixture between F127 and P123, the hydrothermal temperature and time. Briefly, an aqueous solution of polymers was prepared in hydrochloric acid in distilled water overnight. Then, TEOS was added to the mixture at 35 °C under vigorous stirring for 15 minutes until it was completely dissolved. After this, the mixture was placed in an oven for 24 h under static conditions at 35 °C and the mixture was further maintained at 80 °C or 100 °C for hydrothermal treatment during different periods. Subsequently, the samples were calcined at 823 K for 6 hours. The samples are designated as SBA-16-X-*T*-*t*, were X (A, B, C) stands for the composition of the mixture of polymers, *T* is the hydrothermal temperature and *t* is the hydrothermal treatment time.

The starting molar composition was 0.0040F127 : 1.0TEOS : 4.0HCl : 130H_2O for SBA-16 A; 0.00084P1230 : 0038F127 : 1.0TEOS : 4.2HCl : 137H_2O for SBA-16 B, and 0.0016P123 : 0.0037 : 1.0TEOS : 4.4HCl : 144H_2O for SBA-16 C.

Functionalization of the silica surface with *n*-propyl

Functionalization was conducted following the procedure described by Shakeri *et al.*[16a] 700 mg of m-MFC or SBA-16 was dried for 5 h at 140 °C to remove physisorbed water. Then, the solid was dispersed in 25 mL of dry toluene, and 2.5 mL of *n*-propyl triethoxysilane was added to the mixture dropwise over 5 minutes under vigorous stirring, followed by the addition of 1 mL of *n*-butylamine. The mixture was heated to 110 °C and stirred for 48 hours under nitrogen. The obtained materials were filtered off and washed with toluene, toluene : ethanol (1 : 1) and ethanol, and dried at 60 °C for 24 hours. The functionalized materials are named by placing the letter F in front of the silica material's name.

Functionalization of the silica surface with different organosilanes (entrance size determination)

In this procedure, 100 mg of m-MCF or SBA-16 was dried at 140 °C for 5 h to remove physisorbed water. Then, the solid was dispersed in 3.5 mL of dry toluene and 1.72 mmol of organosilane with different carbon lengths was added, followed by the addition of 0.15 mL of *n*-butylamine. The mixture was heated to 110 °C and kept under stirring for 48 hours under nitrogen. The obtained materials were filtered off and washed with toluene, toluene : ethanol (1 : 1) and ethanol, and dried at 60 °C for 24 hours.

Ship in a bottle synthesis. This procedure was conducted *via* a method described by our group recently.[15] The *n*-propyl functionalized m-MCF or SBA-16 (700 mg) was dried at 120 °C for 6 hours under vacuum (−1.0 bar). Then, 150 mg of 3,5-di-*tert*-butyl-2-hydroxybenzaldehyde was dissolved in 2 mL of CH_2Cl_2 and added to the solid. The mixture was kept under stirring for 2 days under reflux at 40 °C under a N_2 atmosphere. Then, 37 mg of (1*R*,2*R*)-diaminocyclohexane was added to the mixture. The mixture was stirred again for 2 days at 40 °C under a N_2 atmosphere. After this period, the solvent was removed by static vacuum. Then, 175.21 mg (2 equiv.) of $FeCl_3{\cdot}6H_2O$ was dissolved in 3 mL of methanol and added to the solid. The system was stirred at RT for 24 h. The mixture was centrifuged (4000 rpm, 5 min) and the solvent was removed by decantation. The remaining solid was washed with toluene (40 mL), methanol (40 mL) and CH_2Cl_2 (40 mL) to remove the unconfined Fe-salen complex. The solids thus obtained were dried under vacuum at 40 °C. The functionalized materials with Fe-salen inside their structure are named by placing the term Fe in front of the silica material's name. For example, Fe-F-m-MCF-60 is the functionalized m-MCF-60 containing the Fe-salen complex in its cage.

Fe(salen) complex synthesis. The synthesis of the salen ligand was done following the procedure described by Jacobsen *et al.*[20] Briefly, a 100 mL three-necked flask was equipped with a cooler, and 78.30 mg (0.686 mmol) of (1*R*,2*R*)-diaminocyclohexane, 189.55 mg (1.37 mmol) of K_2CO_3 and 2.5 mL of distilled H_2O were added. The mixture was stirred until the dissolution of the chemicals, and then 9.5 mL of EtOH was added to the flask. The mixture was heated under stirring to 77 °C, then 321.39 mg (1.37 mmol) of 3,5-di-*tert*-butyl-2-hydroxybenzaldehyde was dissolved in 5 mL of EtOH, added dropwise to the mixture and stirred for 2 h. After that, 2 mL of water was added and the reaction mixture was cooled to a temperature around 5 °C over 2 hours and kept at that temperature for additional 1 hour. Crude solids were obtained by vacuum filtration and washed twice with 2 mL of EtOH. The solids were collected and dissolved in 8 mL of DCM, and washed twice with 5 mL of H_2O and once with 2 mL of brine. The organic layer was dried over Na_2SO_4; the final product was obtained after removal of the solvent using a rotavap. Yield: 72.2% (270.97 mg). IR (KBr pellet): 2960 cm^{-1} ($(CH_3)_3C$–), 2864 cm^{-1} (C–H), 1631 cm^{-1} (C═N), 1595 cm^{-1} (C═C Aromatic). ESI-MS found *m/z*: 547.42.

Complexation of salen with iron was done following a procedure reported previously.[21] 104.61 mg (0.387 mmol) of $FeCl_3{\cdot}6H_2O$ dissolved in 4 ml of MeOH were added to 211.79 mg (0.387 mmol) of ligand dispersed in 2 mL of MeOH. The mixture was stirred for 24 h at room temperature. After this period, a purple solid was collected and washed with MeOH, dissolved in dichloromethane (DCM) and dried over Na_2SO_4. The solution was left to stand at room temperature and crystals were obtained. IR (KBr pallet): 2960 cm^{-1} ($(CH_3)_3C$), 2866 cm^{-1} (C–H), 1602 cm^{-1} (C═N). UV-vis: λ (nm) = 229, 274 (Ar, π–π*), 351 (C═N, π–π*), 514 (Fe, d–d). ESI-MS found *m/z*: 638.71.

Sulfoxidation procedure

Synthesis of iodosylbenzene (PhIO). The synthesis was based on Saltzman *et al.*[22] Briefly, 4.025 g (12.5 mmol) of (diacetoxyiodo) benzene was added to aqueous NaOH (3 M, 18.75 mL) over a period of 5 min. The lumps of solids formed were triturated over a period of 15 min and the reaction mixture was stirred for another 45 min. Then, 12.5 mL of H_2O was added to the solution and the mixture was left to stir for 30–45 min. Büchner filtration was applied to obtain greenish solids. The solids were returned to the beaker and triturated in 50 mL of H_2O, followed by another Büchner filtration. A final purification was done by trituration of the solids in 18.25 mL of chloroform. Green solids were obtained by Büchner filtration; the solids were dried under nitrogen.

Sulfoxidation

The Fe(salen)-based catalyst (1 or 2 mol% relative to thioether) was charged in a glass vial together with 4 mL of solvent and 0.4 mmol of thioether, followed by the addition of an oxidant (0.64 mmol). The mixture was stirred for the desired time and temperature. After this period, the solids were recovered by centrifugation (5 min, 4000 rpm), and the liquid layer was tapped off and analyzed by GC to determine the conversion; the ee values were obtained by HPLC analysis. For recycle experiments, the solid catalysts were recovered by filtration, washed with ethanol (35 mL) and dried under vacuum, and then, the new solution mixture described above was added to the solid.

Instrumentation

GC analysis. A small fraction of the liquid samples was taken and diluted with toluene and analyzed by GC-FID. GC analysis was performed using a PerkinElmer Clarus 500, equipped with a 30 m capillary column with 5% phenyl/95% methylpolysiloxane as the stationary phase (AT5), using the following parameters: initial temperature 50 °C, temperature ramp 10 °C min^{-1}, final temperature 250 °C, injection volume 0.5 μL.

HPLC analysis. All of the chiral HPLC experiments were carried out using a Perkin Elmer Series 200 pump/diode array detector. A chiralcel OD column of 250 × 4.6 mm was used, with a bulk stationary phase consisting of 10 μm particles of the silica support physically coated with the polymeric chiral selector cellulose tris(3,5-dimethylphenylcarbamate). A flow of 1 mL min^{-1} of 80% hexane and 20% isopropanol was used for all experiments.

Electron microscopy. The morphology and sizes of the silica particles were determined with a Tecnai FEI XL 30SFEG scanning electron microscope (SEM). Transmission electron microscopy was performed using a FEI Tecnai20F, operated at 200 kV and equipped with a CCD camera.

The samples were embedded in epoxy resin (Epofix, EMS) and cured at 60 °C overnight. Then, they were cut into thin sections with a nominal thickness of 60 nm using a Diatome Ultra knife, 4 mm wide and 35° clearance angle, mounted on

a Reichert-Jung Ultracut E microtome. The sections floating on water after cutting were picked up and deposited onto a carbon coated polymer grid and left to dry.

Gas physisorption. N_2 and Ar physisorption measurements were performed at 77 K using a Micromeritics Tristar 3000. The samples were dried before the measurement under an N_2 flow at 250 °C for at least 12 h. The functionalized samples were dried at 130 °C for at least 12 h. The micropore and mesopore volumes (V_p) were determined using the *t*-plot method. The pore size distribution of the mesoporous silica supports was calculated from the adsorption branch of the isotherm by BJH analysis. The maximum of the pore size distribution was taken as the average pore diameter.

Elemental analysis. Fe contents of silica was determined by inductively coupled plasma-atomic emission spectroscopy (ICP-AES) using a Metrohm IC Plus 883.

UV-vis and IR spectroscopy. UV-vis experiments were carried out on a Varian Cary 500 Scan UV-vis-NIR spectrophotometer with the configuration in the range of 200–800 nm with a data interval of 1 nm and at a rate of 600 nm min^{-1}.

KBr pellets were prepared by mixing 15 mg of sample with 250 mg of KBr; this mixture was ground into a fine powder, after which it was introduced to a pellet press. The solid was pressured by a 15.011 SPECAC hydraulic press to obtain the KBr pellets. The IR spectroscopic experiments were carried out on a Perkin Elmer Spectrum One FT-IR infrared spectrometer.

TGA analysis. Thermogravimetric analysis (TGA) was carried out using a Perkin-Elmer Pyris 1, with a typical sample quantity of 5 mg and an air flow of 10 ml min^{-1}. A heating rate of 5 °C min^{-1} from 50 °C until 700 °C was used.

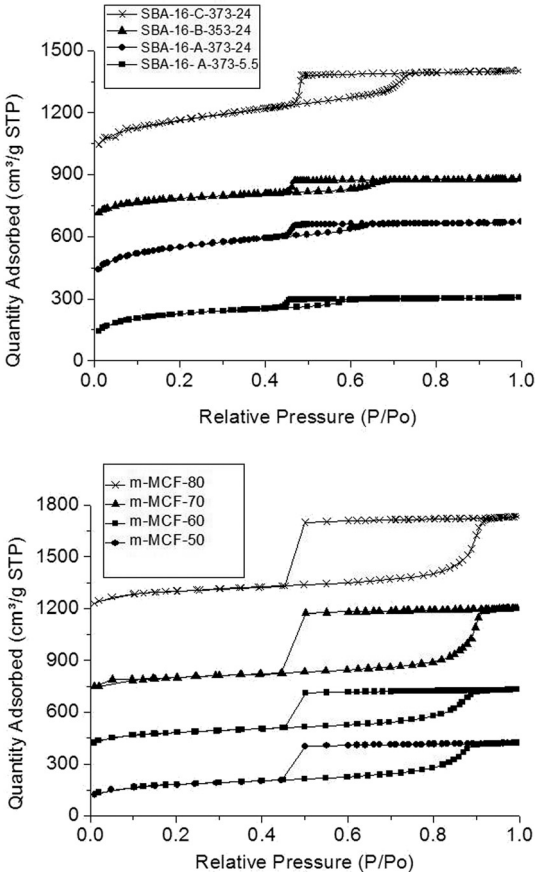

Fig. 1 Nitrogen adsorption isotherms for pristine SBA-16 (top frame) and m-MCF (bottom frame). The isotherms were offset vertically by 300, 600 and 900 for the SBA-16 materials and by 300, 600, and 1100 for m-MCF.

Results and discussion

Synthesis and pretreatment of mesoporous materials

The N_2 physisorption isotherms of the pristine ordered mesoporous materials (m-MCF and SBA-16) are displayed in Fig. 1. The isotherms can be classified as type IV following the IUPAC classification since they show one step capillary condensation in the adsorption branch (Fig. 1), corresponding to the filling of the uniform mesopores by N_2 molecules. In all cases, ink-bottle hysteresis was observed, showing that liquid N_2 remained trapped by the narrow entrances of the pores, resulting in delayed desorption at a relative pressure around 0.45. This fact does not permit the exact determination of the entrance sizes of these materials since liquid nitrogen is not stable below a relative pressure of 0.45.

Argon physisorption at 77 K is an alternative technique to study the entrance size of these materials due to the capillary evaporation of argon which takes place at lower relative pressures than with nitrogen thus extending its use to analyze entrance sizes down to 3.8 nm. The argon physisorption isotherms of the synthesized materials are shown in Fig. 2. From the obtained hysteresis of the synthesized m-MCF and SBA-16, it is possible to conclude that the majority of entrance sizes are smaller than 3.8 nm. However, the sample SBA-16-C-373-24 showed a small fraction of entrance sizes around 3.8 nm (see material designations in the Experimental section).

A method based on the post-synthetic functionalization of the silica surface with alkoxysilanes with different carbon chain lengths was applied for determining the entrance size of the synthesized materials.[16] After this functionalization, the obtained hybrid materials were examined by nitrogen physisorption to study the accessibility of the pores for N_2 molecules; see the ESI† for details (Fig. S1 and S2 show the isotherms of the synthesized materials after the functionalization with different organosilanes) and the derived values of entrance size in Table 1.

Table 1 shows the structural properties of the synthesized silica materials (m-MCF and SBA-16). The increase of cage size resulted almost always in an increase of the entrance size especially for the SBA-16 materials. However, we were able to reduce the entrance sizes of the SBA-16 materials by decreasing the hydrothermal treatment time, in good agreement with the results reported by Li *et al.*[14a] and Jaroniec *et al.*[16b] The obtained materials were examined by SEM (ESI† Fig. S3 and S4) and TEM (Fig. 3) to assess the ordered structure of pristine SBA-16 and m-MCF.

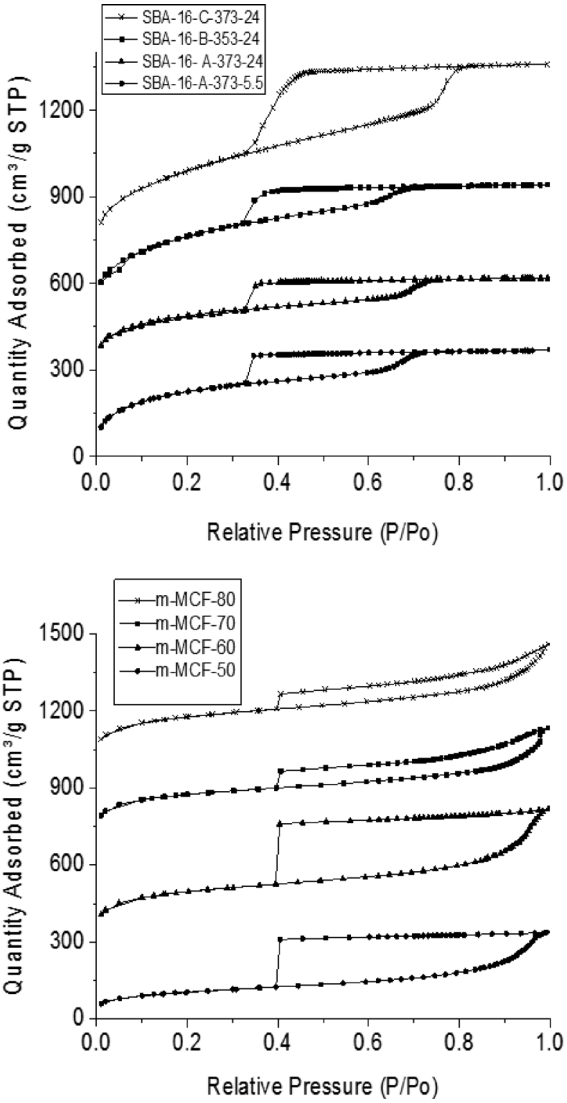

Fig. 2 Argon adsorption isotherms for pristine SBA-16 (top frame) and m-MCF (bottom frame). The isotherms were offset vertically by 300, 500 and 700 for the SBA-16 materials and by 300, 700, and 1000 for m-MCF.

Table 1 Structural properties of pristine materials from N_2 physisorption and surface modification; for material designations see the Experimental section

Material	Surface area (m^2 g^{-1})	Pore volume (cm^3 g^{-1})	Cage size[a] (nm)	Entrance size[b] (nm)
SBA-16-A-373-5.5	769	0.49	5.0	2.0
SBA-16-A-373-24	875	0.56	5.0	2.5
SBA-16-B-353-24	634	0.43	6.5	2.8
SBA-16-C-373-24	911	0.77	7.5	3.2
m-MCF-50	619	0.65	16	2.0
m-MCF-60	623	0.66	16.5	2.0
m-MCF-70	685	0.92	20.8	2.5
m-MCF-80	689	0.96	21.2	2.8

[a] Determined by BJH analysis from the adsorption branch. [b] Determined by post-synthetic treatments.

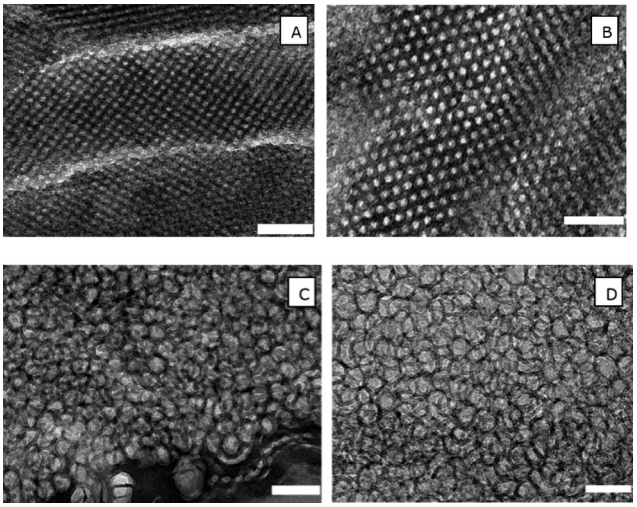

Fig. 3 TEM images of pristine host materials: (A) SBA-16-B-353-24, (B) SBA-16-C-373-24, (C) MCF-50, and (D) MCF-70. All scale = 50 nm.

Preparation and characterization of catalysts

A post synthetic functionalization with *n*-propyl groups of silica materials (Table 2) was carried with the intention of narrowing the entrance sizes and allowing a better dispersion of solid materials in organic solvents (ESI† Fig. S5) due to the increase of hydrophobicity (organic solvents are commonly used as solvents for salen complex synthesis and as solvents for sulfoxidation reactions). Moreover, the functionalization decreases the acidity of silica that might cause the degradation of the trapped salen complex. After the functionalization, N_2 physisorption was used to characterize these materials (Table 2), showing a decrease of the porosity, surface area and pore size compared to pristine SBA-16 and m-MCF (isotherms in the ESI,† Fig. S6).

IR spectroscopy was used to assess the presence of alkyl groups on silica. The peaks at 2850–2970 cm^{-1} which correspond to the C–H stretch vibrations of alkyl groups were observed. Moreover, the intensity of the peak at 3740 cm^{-1} which corresponds to the stretching mode of free silanol groups almost disappeared (ESI,† Fig. S7), showing the successful grafting of the organosilanes on the silica surface. TGA analyses were used to confirm the decomposition of alkyl groups grafted on the silica surface (ESI,† Fig. S8), suggesting the successful functionalization of the external and internal walls of the silica (the functionalized materials are designated as F-m-MCF and F-SBA-16).

A salen ligand was selected as a model which allows us to obtain reasonable loadings in the cages of different materials.[14a,14b,15] Scheme 1 shows the reaction (Schiff base reaction) which took place inside the cage structure of F-m-MCF and F-SBA-16 (for more details, see the Experimental section). IR spectroscopy was used to confirm the formation of the salen ligand inside m-MCF-60, as a new peak at 1632 cm^{-1} appeared which corresponds to C=N bond formation (Fig. 4B) and the absence of the peaks at 1582 cm^{-1} and 1760 cm^{-1} which correspond to primary amine and carbonyl

Table 2 Structural properties of functionalized mesoporous materials from N_2 physisorption (designated as F-m-MCF and F-SBA-16 materials)

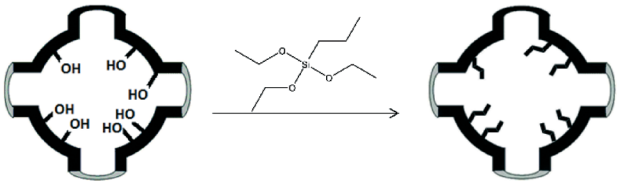

Material	Surface area ($m^2\ g^{-1}$)	Pore volume ($cm^3\ g^{-1}$)	Cage size[a] (nm)
F-SBA-16-A-373-5.5	368	0.23	4.3
F-SBA-16-A-373-24	455	0.29	4.5
F-SBA-16-B-353-24	341	0.24	5.3
F-SBA-16-C-373-24	500	0.40	6.8
F-m-MCF-50	332	0.43	14
F-m-MCF-60	313	0.41	16
F-m-MCF-70	379	0.64	21
F-m-MCF-80	376	0.65	21

[a] Determined by BJH analysis from the adsorption branch.

groups of aldehyde in the spectrum, confirming the successful formation and encapsulation of the salen ligand in m-MCF-60.

Upon complexation with iron, a color change from yellow to red was observed in the solid material, giving a strong indication that the Fe(salen) complex was formed inside functionalized m-MCF and SBA-16. The UV-vis spectra of all materials (m-MCF and SBA-16) are shown in Fig. 6. In almost all cases, four bands were observed; the bands at 220 and 280 nm are attributed to π–π* located predominantly on the phenyl ring and the peak at 312–350 nm to C═N.[17,9f] The expected d–d transition at 522–565 nm of Fe(salen) was also observed, further confirming its formation inside the silica materials (the materials were designated as Fe-F-m-MCF and Fe-F-SBA-16). The homogeneous complex was also synthesized and physically mixed with m-MCF-60; this mixture showed the same peaks as those observed for materials synthesized by the "ship in the bottle" approach (Fig. 5). The isotherms from N_2 physisorption at 77 K of pristine m-MCF-60, F-m-MCF-60 and Fe-F-m-MCF-60 are shown in the ESI† (Fig. S9).

The intensities of the characteristic bands of Fe(salen) decreased with the increase of the pore entrance sizes. These intensities are related to their concentration inside the silica structures (Fig. 6). In the case of F-SBA-16-C-373-24 which has an entrance size around 3.2 nm, no characteristic UV-vis bands were observed, suggesting no encapsulation of the complex, due to the large entrance size. A higher concentration of salen complex inside the materials is observed when the entrance sizes are smaller than 2 nm (F-m-MCF-50, F-m-MCF-60 and F-SBA-16-A-5.5). Table 3 shows the iron content in the materials measured by inductively coupled plasma (ICP) which is in line with the UV-vis spectra results. In general, a higher concentration of Fe(salen) complexes is encapsulated in the m-MCF materials than in the SBA-16 materials. For example, m-MCF-50 contained 4 times more iron than F-SBA-16-A-373-5.5, showing the advantages of m-MCF for this approach.

The IR spectrum of F-m-MCF-60 after complexation of iron is shown in Fig. 4A. It is known that the band which corresponds to C═N displays a red-shift of 3–12 cm^{-1} after complexation, which corresponds to the participation of the azomethine and phenolic oxygen of the ligand binding to Fe ions.[17a] However, only a part of this band shows this shift in the studied case, indicating an incomplete complexation of Fe with the salen ligand; in other words, not all salen ligands present in m-MCF-60 participate in the complexation of iron.

Asymmetric oxidation of sulfides

The asymmetric oxidation of thioanisole was used as a model reaction (Table 4). This reaction was run in different solvents, using different oxidants, and Fe(salen) immobilized on F-m-MCF-60 or pure Fe(salen) as catalysts. In all cases, a high selectivity to methylsulfinyl-benzene (Table 4, **1a**) was observed with a very small fraction of the substrate being further oxidized to methylsulfonyl-benzene (**1b**). Iodosylbenzene (PhIO) was the only oxidant which gave rise to enantioselectivity, in agreement with the results reported by Talsi *et al.* that the Fe(salen) complex is able to form specific active sites with PhIO by a Lewis acid activation of iodosylbenzene to form the oxygen-transfer species.[6] A blank reaction was also run under the same conditions reported in Table 4, entry 12, using F-MCF-60 without the iron complex inside the cages; only 3% of thioanisole was converted.

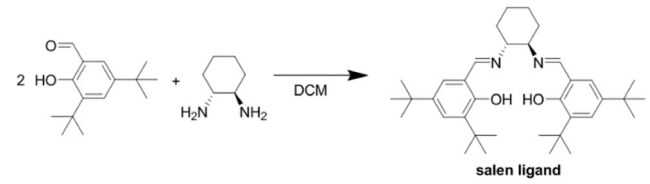

Scheme 1 Schiff base reaction which takes place inside the cages of the synthesized materials.

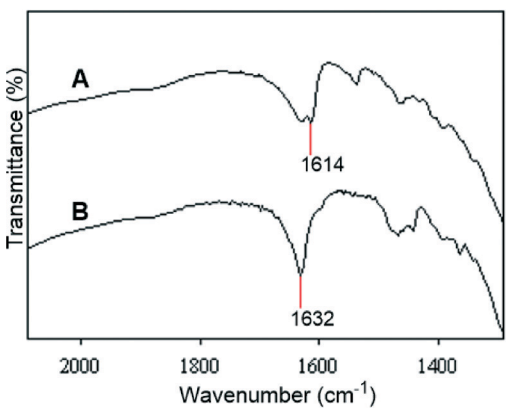

Fig. 4 IR spectra of: A) Fe-F-m-MCF-60 and B) the salen ligand immobilized on F-m-MCF-60.

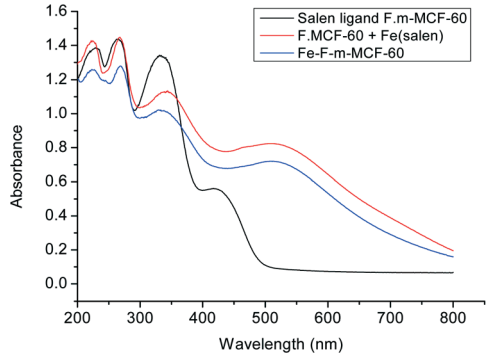

Fig. 5 UV-vis spectra of the salen ligand encapsulated or Fe(salen) encapsulated in m-MCF-60 and the physical mixture of Fe(salen) with F-m-MCF-60.

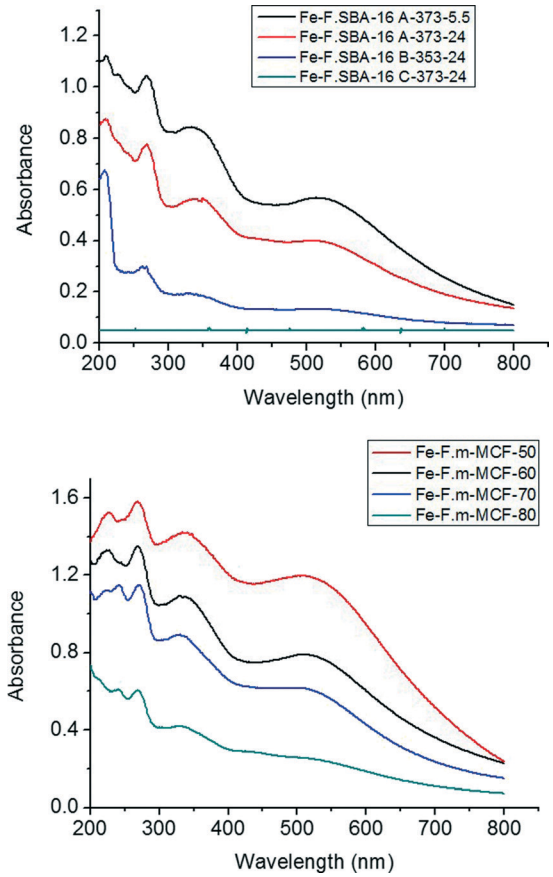

Fig. 6 UV-vis spectra of the Fe(salen) complex immobilized on cage-like materials based on F-SBA-16 and F-m-MCF.

If acetonitrile and dichloromethane were used as solvents, low conversions of thioanisole were observed when PhIO was used as an oxidant. On the other hand, the conversion was higher using H_2O_2 (Table 4, entries 2, 4, 5, and 8), which is probably related to the limited solubility of PhIO in these solvents. Thus, methanol was selected as a solvent due to the higher solubility of PhIO. In this case, a remarkable increase of the conversion was observed (Table 4, entry 12). Sodium hypochlorite was also used as an oxidizing agent, but low conversions were observed as was reported before for sulfoxidation of thioanisole using a homogeneous Fe(salen) complex as a catalyst.[6]

Table 3 Iron loading in the synthesized materials

Material	Fe loading (w/w)%
Fe-F-SBA-16-A-373-5.5	0.19
Fe-F-SBA-16-A-373-24	0.14
Fe-F-SBA-16-B-353-24	0.06
Fe-F-SBA-16-C-373-24	<0.005
Fe-F-m-MCF-50	0.85
Fe-F-m-MCF-60	0.70
Fe-F-m-MCF-70	0.50
Fe-F-m-MCF-80	0.26

The comparison between the activity of the Fe(salen) complex immobilized on F-m-MCF and F-SBA-16 was also explored. Despite the same entrance sizes, higher conversion values were observed when the Fe(salen) complex was immobilized on F-m-MCF (Table 5, entries 2–9), probably the large cage sizes of these materials allow more freely moving Fe(salen) complexes with concomitant higher activities. The conversions observed with the larger substrate benzyl phenyl sulfide were considerably lower in the case of F-SBA-16, F-m-MCF-50 and F-m-MCF-60 when compared to F-m-MCF-70 and F-m-MCF-80. Probably, the combination of larger cages and in particular entrance sizes of F-m-MCF-70 and F-m-MCF-80 facilitates the diffusion of this substrate and PhIO, producing a more suitable catalyst. Moreover, even for the catalyst based on F-m-MCF-70 and F-m-MCF-80, the oxidation of benzyl phenyl sulfide was slightly lower than the conversion of thioanisole. This data shows that the conversion values can be optimized through tuning the silica structure (entrance size and cage size).

The homogeneous Fe(salen) complex was also tested as a catalyst for comparison (Table 4, entries 1, 7, and 9). The homogeneous counterpart showed only slightly higher activity than the immobilized complex in the cages of F-m-MCF-60 for thioanisole as a substrate. This is much more favorable than some results previously reported;[18] for example, Ogunwumi *et al.* reported that an immobilized Mn salen complex on zeolites suffered large reduction of the activity when compared with homogeneous counterparts.[13c] Table 4 also shows that the homogeneous catalyst presented somewhat higher enantioselectivity when compared to immobilized systems.

To determine the nature of the catalytic species for the reaction, a hot filtration test was performed for the oxidation of thioanisole using Fe(salen) immobilized on F-m-MCF-60 as a catalyst; after 1 hour of reaction the liquid and solid phases were separated. The liquid phase was kept under the same reaction conditions, showing that the filtrate was only able to provide a slight additional conversion of around 5% (Fig. 7). This gives a strong indication that the vast majority of the reaction is catalyzed by iron (salen) inside the m-MCF structure. A hot filtration test was also run using Fe-F-m-MCF-70 with benzyl phenyl sulfide as a substrate (ESI,† Fig. S12).

Table 4 Oxidation of thioanisole using Fe(salen) or Fe(salen) immobilized on F-m-MCF-60 with different solvents and oxidants

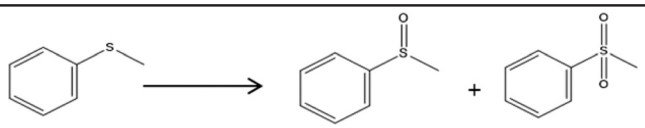

1a **1b**

Entry	Solvent	Oxidant	Conversion[a] (%)	Selectivity[b] (%)	ee[c] (%)
1[d]	CH_3CN	PhIO	68	99	64
2	CH_3CN	H_2O_2	65	99	0
3	CH_3CN	NaOCl	8	98	0
4	CH_3CN	PhIO	11	99	55
5	CH_2Cl_2	H_2O_2	40	99	0
6	CH_2Cl_2	NaOCl	8	99	0
7[d]	CH_2Cl_2	PhIO	65	99	60
8	CH_2Cl_2	PhIO	10	99	56
9[d]	CH_3OH	PhIO	92	98	66
10	CH_3OH	H_2O_2	94	95	0
11	CH_3OH	NaOCl	20	98	0
12	CH_3OH	PhIO	90	98	57
13[e]	CH_3OH	PhIO	65	99	62

[a] Determined with GC-FID. [b] Selectivity to **1a**. [c] Determined by chiral HPLC analysis. [d] Homogeneous Fe(III) salen complex used as a catalyst. [e] The reaction was run at 0 °C for 10 hours. Reaction conditions: 4 mL of solvent, 0.4 mmol of thioanisole, oxidant (0.65 mmol) and catalyst (1 mol% Fe), 20 °C, 4 hours.

Table 5 Sulfoxidation using Fe(salen) and Fe(salen) immobilized on F-m-MCF and SBA-16

Entry	Material	Substrate	Conversion[a] (%)	Selectivity[b] (%)	ee[c] (%)
1	Fe-salen complex	PhSMe	92	98	66
2	Fe-F-m-MCF-50	PhSMe	92	97	58
3	Fe-F-m-MCF-60	PhSMe	90	98	57
4	Fe-F-SBA-16-A-373-5.5	PhSMe	60	98	55
5	Fe-F-m-MCF-70	PhSMe	91	97	55
6	Fe-F-SBA-16-A-373-24	PhSMe	65	98	56
7	Fe-F-m-MCF-80	PhSMe	90	98	56
8	Fe-F-SBA-16-B-353-24	PhSMe	67	98	57
9	Fe-F-SBA-16-C-373-24	PhSMe	4	98	0
10	Fe-salen complex	$PhCH_2SPh$	94	98	74
11	Fe-F-m-MCF-50	$PhCH_2SPh$	39	94	60
12	Fe-F-m-MCF-60	$PhCH_2SPh$	43	93	62
13	Fe-F-SBA-16-A-373-5.5	$PhCH_2SPh$	25	98	60
14	Fe-F-m-MCF-70	$PhCH_2SPh$	80	95	63
15	Fe-F-SBA-16 A-373-24	$PhCH_2SPh$	40	98	61
16	Fe-F-m-MCF-80	$PhCH_2SPh$	82	95	64
17	Fe-F-SBA-16-B-353-24	$PhCH_2SPh$	60	96	65
18	Fe-F-SBA-16-C-373-24	$PhCH_2SPh$	2	99	0

[a] Determined with GC-FID. [b] Selectivity to the corresponding sulfoxide. [c] Determined by chiral HPLC analysis. Reaction conditions: 4 mL of MeOH, 0.4 mmol of substrate, PhIO (0.65 mmol), catalyst (1 mol% Fe), 20 °C, 4 hours.

The recyclability of Fe(salen)F-m-MCF-70 was investigated in the asymmetric oxidation of benzyl phenyl sulfide using PhIO as an oxidant and methanol as solvent (Table 6). This reaction was selected due to the higher enantioselectivity obtained when compared to the values obtained for thioanisole. The catalyst was recovered by filtration and washed thoroughly with ethanol. The catalyst could be recycled two times without loss of activity and chemical selectivity, but a slight decrease of enantioselectivity was apparent. However, a slight loss of catalytic activity was observed during the third cycle. The content of iron was determined to investigate the possible explanation for this deactivation; however, the leaching of iron was insignificant. The recyclability of thioanisole was also run and is shown in Table S2 (ESI†).

UV-vis spectroscopy was used to study any possible change in the Fe(salen) complex structure inside F-m-MCF-70. Fig. 8 shows that the reused catalyst (after three cycles) still presents two bands at 200–300 nm which correspond to π–π^* of the phenyl ring; however, the band at 350 nm which is attributed to C=N cannot be seen anymore, giving a strong

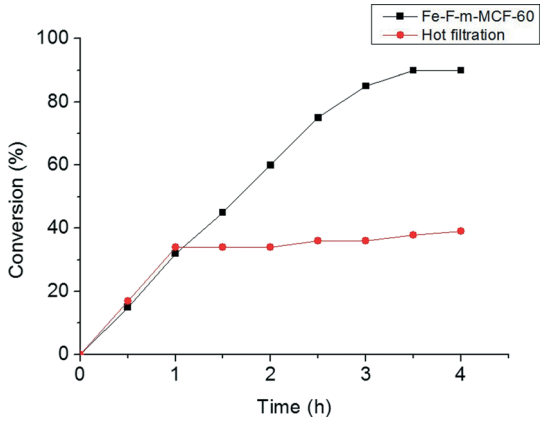

Fig. 7 Time–conversion plot and leaching test as evidence for the nature of the catalyst for the sulfoxidation of thioanisole.

Table 6 Recyclability of Fe(salen) immobilized on F-m-MCF-70 for the oxidation of benzyl phenyl sulfide

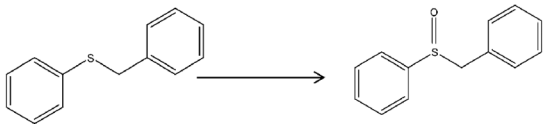

Run	Conversion[a] (%)	Selectivity[b] (%)	ee[c] (%)
1	80	95	63
2	79	97	55
3	61	98	0
4	60	98	0
5	52	98	0

[a] Determined with GC-FID. [b] Selectivity to the corresponding sulfoxide. [c] Determined by chiral HPLC analysis. Reaction conditions: 4 mL of MeOH, 0.4 mmol of benzyl phenyl sulfide, PhIO (0.65 mmol), catalyst (2 mol%), 20 °C, 4 hours.

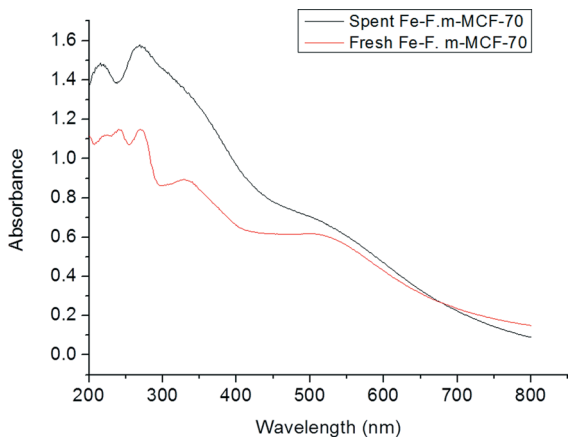

Fig. 8 UV-vis spectra of fresh and reused Fe(salen) complexes encapsulated in F-m-MCF-70.

indication that the Fe(salen) complex suffered changes in its molecular structure. Moreover, the band which corresponds to the d–d transition at 522–565 nm of Fe(salen) is not so well-defined, probably due to a possible decomposition of encapsulated Fe(salen) and the formation of iron oxide particles, since the presence of these particles was suggested by XRD analysis as a broad peak was observed around 50° two-theta (ESI,† Fig. S10).

Conclusions

A chiral Fe(salen) complex was encapsulated in the nanocages of *n*-propyl modified SBA-16 and m-MCF. The silica structure (entrance and cage sizes) was important to determine the final loadings of Fe(salen) inside these materials. In general, the structure of m-MCF materials provides a higher loading of Fe(salen) complexes compared to SBA-16, probably due to their larger cage sizes. The catalytic activity of the materials could be tuned by changing the entrance and cage dimensions of the silica structure, and adjusting them to the specific substrate used. For the catalytic performance, the enantioselectivity of sulfoxidation reactions was just observed when PhIO was used as an oxidant as previously reported for the homogenous complex.[6] Moreover, Fe(salen) trapped in the mesoporous materials showed almost the same activity and enantioselectivity as the homogeneous counterpart. During recyclability tests, the immobilized complex showed deactivation after the second cycle, related to the decomposition of the encapsulated Fe(salen) complex and the formation of iron oxide particles.

Acknowledgements

The authors acknowledge support from European Research Council (ERC) advanced grant no. 338846, the Dutch National Research School Combination Catalysis (NRSCC) and São Paulo Research Foundation grant no. 2015/07773-0. The authors would also like to thank Allan Ribeiro da Silva for NMR measurement.

Notes and references

1 (*a*) I. Fernández and N. Khiar, *Chem. Rev.*, 2003, **103**, 3651; (*b*) E. Wojaczyńska and J. Wojaczyński, *Chem. Rev.*, 2010, **110**, 4303; (*c*) M. C. Carreno, *Chem. Rev.*, 1995, **95**, 1717–1760.

2 (*a*) R. Bentley, *Chem. Soc. Rev.*, 2005, **34**, 609; (*b*) J. Legros, J. Dehli and C. Bolm, *Adv. Synth. Catal.*, 2005, **347**, 19; (*c*) S. Morita, J. Matsubara, K. Otsubo, K. Kitano, T. Ohtani, Y. Kawano and M. Uchida, *Tetrahedron*, 1997, **8**, 3707; (*d*) S. Padmanabhan, R. C. Lavin and G. J. Durant, *Tetrahedron*, 2000, **11**, 3455; (*e*) H. Pellissier, *Tetrahedron*, 2006, **62**, 5559.

3 (*a*) X. Gu, X. Li, Y. Chai, Q. Yang, P. Li and Y. Yao, *Green Chem.*, 2013, **15**, 357; (*b*) F. Voss, E. Herdtweck and T. Bach, *Chem. Commun.*, 2011, **47**, 2137; (*c*) G. E. O'Mahony, A. Ford and A. R. Maguire, *J. Sulfur Chem.*, 2013, **34**, 301; (*d*) J. Dad'ová, E. Svobodová, M. Sikorski, B. König and R. Cibulka, *ChemCatChem*, 2012, **4**, 620; (*e*) K. Matsumoto, T. Yamaguchi, J. Fujisaki, B. Saito and T. Katsuki, *Chem. – Asian J.*, 2008, **3**, 351; (*f*) A. Lazar, P. Sharma and A. P. Singh, *Microporous Mesoporous Mater.*, 2013, **170**, 331; (*g*) M. R. Maurya, A. K. Chandrakar and S. Chand, *J. Mol. Catal.*

A: Chem., 2007, **263**, 227; (*h*) W. Adam, F. Heckel, C. R. Saha-Möller, M. Taupp and P. Schreier, *Tetrahedron*, 2004, **15**, 983; (*i*) V. V. Thakur and A. Sudalai, *Tetrahedron*, 2003, **14**, 407; (*j*) T. Katsuki, *Synlett*, 2003, **7**, 1046.

4 (*a*) C. Bolm and O. A. G. Dabard, *Synlett*, 1999, **5**, 360; (*b*) C. Bolm and F. Bienewald, *Synlett*, 1998, 1327; (*c*) S. Barroso, F. Madeira, M. J. Calhorda, M. J. Ferreira, M. T. Duarte and A. M. Martins, *Inorg. Chem.*, 2013, **52**, 9427; (*d*) S. Barroso, P. Adão, F. Madeira, M. T. Duarte, J. C. Pessoa and A. M. Martins, *Inorg. Chem.*, 2010, **49**, 7452; (*e*) J. Brinksma, B. L. Feringa, R. Hage and J. Kerschner, *Chem. Commun.*, 2000, 537; (*f*) A. R. Silva, V. Budarin and J. H. Clark, *ChemCatChem*, 2013, **5**, 895; (*g*) M. Matsugi, N. Fukuda, Y. Muguruma, T. Yamaguchi and J. Minamikawa, *Tetrahedron*, 2001, **57**, 2739; (*h*) T. Kataukp, *Tetrahedron Lett.*, 1994, **35**, 1887; (*i*) Q. Zeng, Y. Gao, J. Dong, W. Weng and Y. Zhao, *Tetrahedron*, 2011, **22**, 717; (*j*) C. Kokubo and T. Katsuki, *Tetrahedron*, 1996, **52**, 13895; (*k*) S. Schoumacker, O. Hamelin, J. Pécaut and M. Fontecave, *Inorg. Chem.*, 2003, **42**, 8110.

5 (*a*) K. P. Bryliakov and E. P. Talsi, *Chemistry*, 2007, **13**, 8045; (*b*) J. Legros and C. Bolm, *Angew. Chem., Int. Ed.*, 2004, **43**, 4225; (*c*) J. Legros and C. Bolm, *Angew. Chem., Int. Ed.*, 2003, **42**, 5487; (*d*) J. Legros and C. Bolm, *Chemistry*, 2005, **11**, 1086; (*e*) L. Villalobos and T. Ren, *Inorg. Chem. Commun.*, 2013, **28**, 52; (*f*) B. Li, A.-H. Liu, L.-N. He, Z.-Z. Yang, J. Gao and K.-H. Chen, *Green Chem.*, 2012, **14**, 130; (*g*) J. Park, Y. Morimoto, Y.-M. Lee, W. Nam and S. Fukuzumi, *Inorg. Chem.*, 2014, **53**, 3618; (*h*) S. Liao and B. List, *Adv. Synth. Catal.*, 2012, **354**, 2363.

6 K. P. Bryliakov and E. P. Talsi, *Angew. Chem., Int. Ed.*, 2004, **43**, 5228.

7 H. Egami and T. Katsuki, *J. Am. Chem. Soc.*, 2007, **129**, 8940.

8 (*a*) R. L. Oliveira, P. K. Kiyohara and L. M. Rossi, *Green Chem.*, 2009, **11**, 1366; (*b*) R. L. Oliveira, D. Zanchet, P. K. Kiyohara and L. M. Rossi, *Chemistry*, 2011, **17**, 4626; (*c*) R. L. Oliveira, P. K. Kiyohara and L. M. Rossi, *Green Chem.*, 2010, **12**, 144; (*d*) R. L. Oliveira, J. B. F. Hooijmans, P. E. de Jongh, R. J. M. Klein Gebbink and K. P. de Jong, *ChemCatChem*, 2014, **6**, 3223; (*e*) R. L. Oliveira, W. He, R. J. M. K. Gebbink and K. P. de Jong, *Catal. Sci. Technol.*, 2015, **5**, 1919–1928.

9 (*a*) N. Madhavan and M. Weck, *Adv. Synth. Catal.*, 2008, **350**, 419; (*b*) B. Li, S. Bai, P. Wang, H. Yang, Q. Yang and C. Li, *Phys. Chem. Chem. Phys.*, 2011, **13**, 2504; (*c*) L. Canali, E. Cowan, C. L. Gibson, D. C. Sherrington and H. Deleuze, *Chem. Commun.*, 1998, 2561; (*d*) S. Bai, B. Li, J. Peng, X. Zhang, Q. Yang and C. Li, *Chem. Sci.*, 2012, **3**, 2864; (*e*) R. Kureshy, I. Ahmad, N. Khan, S. Abdi, K. Pathak and R. Jasra, *J. Catal.*, 2006, **238**, 134; (*f*) Z. Li, S. Wu, H. Ding, H. Lu, J. Liu, Q. Huo, J. Guan and Q. Kan, *New J. Chem.*, 2013, **37**, 4220; (*g*) C. Baleizao and H. Garcia, *Chem. Rev.*, 2006, **106**, 3987; (*h*) R. J. M. Klein Gebbink and M. A. N. Virboul, in *Enantioselective Homogeneous Supported Catalysis*, ed. R. Sebesta, RSC, 2012, p. 123.

10 (*a*) C. S. Gill, K. Venkatasubbaiah and C. W. Jones, *Adv. Synth. Catal.*, 2009, **351**, 1344; (*b*) C. W. Jones, *Top. Catal.*, 2010, **53**, 942.

11 V. Salinier, G. P. Niccolai, V. Dufaud and J.-M. Basset, *Adv. Synth. Catal.*, 2009, **351**, 2168.

12 (*a*) C. Li, H. Zhang, D. Jiang and Q. Yang, *Chem. Commun.*, 2007, 547; (*b*) A. B. Sorokin, in *Liq. Phase Oxid. via Heterog. Catal. Org. Synth. Ind. Appl.*, 2013, p. 321.

13 (*a*) E. Möllmann, P. Tomlinson and W. Hölderich, *J. Mol. Catal. A: Chem.*, 2003, **206**, 253; (*b*) S. Koner, *Chem. Commun.*, 1998, 593; (*c*) S. B. Ogunwumi and T. Bein, *Chem. Commun.*, 1997, 901; (*d*) F. Bedioui, *Coord. Chem. Rev.*, 1995, **144**, 39; (*e*) J. Sabater, A. Corma, A. Domenech and V. Forn, *Chem. Commun.*, 1997, 1285.

14 (*a*) H. Yang, L. Zhang, W. Su, Q. Yang and C. Li, *J. Catal.*, 2007, **248**, 204; (*b*) M. Shakeri, R. J. M. Klein Gebbink, P. E. de Jongh and K. P. de Jong, *Angew. Chem., Int. Ed.*, 2013, **52**, 10854; (*c*) B. Li, S. Bai, X. Wang, M. Zhong, Q. Yang and C. Li, *Angew. Chem., Int. Ed.*, 2012, **51**, 11517; (*d*) H. Yang, L. Zhang, L. Zhong, Q. Yang and C. Li, *Angew. Chem., Int. Ed.*, 2007, **46**, 6861.

15 M. Shakeri, L. Roiban, V. Yazerski, G. Prieto, J. M. K. Gebbink, P. E. De Jongh and K. P. De Jong, *ACS Catal.*, 2014, **4**, 3791.

16 (*a*) M. Shakeri, R. J. M. Klein Gebbink, P. E. de Jongh and K. P. de Jong, *Microporous Mesoporous Mater.*, 2013, **170**, 340; (*b*) M. Kruk, V. Antochshuk, J. R. Matos, L. P. Mercuri and M. Jaroniec, *J. Am. Chem. Soc.*, 2002, **124**, 768.

17 (*a*) Y. Yang, J. Guan, P. Qiu and Q. Kan, *Transition Met. Chem.*, 2009, **35**, 263; (*b*) S. Soundiressane, S. Selvakumar, O. Ménage, M. Hamelin, A. P. Fontecave and J. Singh, *Mol. Catal. A: Chem.*, 2007, **270**, 132; (*c*) A. Kilic, E. Tas, B. Deveci and I. Yilmaz, *Polyhedron*, 2007, **26**, 4009.

18 (*a*) B. Gigante, A. Corma and H. Garcia, *Catal. Lett.*, 2000, **68**, 113; (*b*) W. Kahlen and H. H. Wagner, *Catal. Lett.*, 1998, **54**, 85.

19 T. Kim, R. Ryoo, M. Kruk, K. P. Gierszal and M. Jaroniec, *J. Phys. Chem. B*, 2004, **108**, 11480.

20 J. F. Larrow, E. N. Jacobsen, Y. Gao, Y. Hong, X. Nie and C. M. Zepp, *J. Organomet. Chem.*, 1994, **4**, 1939.

21 L. Tao, L. Qin-Xuan, R. Wen-Juan, Z. Zhi-Ang and C. Yun-Ti, *Chin. J. Chem.*, 2001, **19**, 352.

22 H. Saltzman and J. G. Sharefkin, *Org. Synth. Coll.*, 1973, **5**, 658.